Molecular Oxygen Induced in-Gap States in PbS Quantum Dots

Yingjie Zhang,[†,‡,#] Danylo Zherebetskyy,[‡,#] Noah D. Bronstein,[§] Sara Barja,[‡] Leonid Lichtenstein,[‡] A. Paul Alivisatos,[‡,§,∥,⊥] Lin-Wang Wang,[‡] and Miquel Salmeron*[,‡,∥]

[†]Applied Science and Technology Graduate Program, [§]Department of Chemistry, and [∥]Department of Materials Science and Engineering, University of California, Berkeley, California 94720, United States, [‡]Materials Sciences Division, Lawrence Berkeley National Laboratory, Berkeley, California 94720, United States, and [⊥]Kavli Energy NanoScience Institute, Berkeley, California 94720, United States. [#]Y. Zhang and D. Zherebetskyy contributed equally to this work.

ABSTRACT Artificial solids composed of semiconductor quantum dots (QDs) are being developed for large-area electronic and optoelectronic applications, but these materials often have defect-induced in-gap states (IGS) of unknown chemical origin. Here we performed scanning probe based spectroscopic analysis and density functional theory calculations to determine the nature of such states and their electronic structure. We found that IGS near the valence band occur frequently in the QDs except when treated with reducing agents. Calculations on various possible defects and chemical spectroscopy revealed that molecular oxygen is most likely at the origin of these IGS. We expect this impurity-induced deep IGS to be a common occurrence in ionic semiconductors, where the intrinsic vacancy defects either do not produce IGS or produce shallow states near band edges. Ionic QDs with surface passivation to block impurity adsorption are thus ideal for high-efficiency optoelectronic device applications.

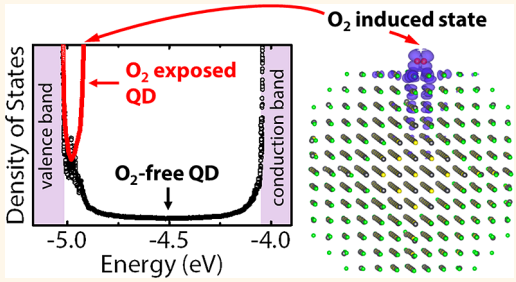

KEYWORDS: PbS quantum dot · nanocrystal · in-gap states · molecular oxygen · defect · scanning probe microscopy · DFT calculation

The evolution of semiconductor electronics and optoelectronics began with the controlled doping of impurity atoms into semiconductor crystals, which opened the way to engineer their charge transport properties.[1] On the other hand, unwanted impurities or defects can hinder transport and limit device performance.[2] The development of nanomaterials of controlled size made it possible to engineer the band gap and tune the electronic properties from the bottom up. As a trade-off, the impact of surface impurities on the electronic properties of nanomaterials is more prominent due to the large surface-to-volume ratio and strong quantum confinement effects.[3−5] For colloidally synthesized nanocrystals or quantum dots in particular, surface-related in-gap states (IGS) are believed to assist the recombination of photoexcited charge carriers,[6] which limits the optoelectronic device efficiency.[7,8] Here we focus on PbS quantum dots (QDs), which have produced the best-performing solar cells.[9−11] Recently, Bawendi *et al.* reported the presence of emissive IGS that form an "effective band" inside the band gap and ~0.2 eV away from the band edge, which were believed to be at the origin of the high open-circuit voltage deficit in the QD solar cells.[12] Remarkably, this is in good agreement with our previous work, where we found a band of IGS ≈ 0.2 eV above the valence band of PbS QDs, which form percolation pathways assisting carrier transport.[13,14] In addition, Sargent *et al.* and Klimov *et al.* found similar IGS using transient absorption and scanning tunneling spectroscopy (STS) methods.[7,8,15]

Although the existence and the energy level of IGS have been established, until now the nature of the IGS is still unclear. Theoretical predictions include nonstoichiometry of the constituent atoms,[16] incomplete ligand passivation,[8] and charge-induced surface reconstruction.[17] The bottleneck for the understanding of IGS is the complicated surface chemistry and ligand passivation structure of the QDs, which makes it difficult to correlate theory with experimental investigations. We overcame this obstacle with a combined effort of state-of-the-art density functional theory (DFT) calculations and chemical spectroscopy on real PbS QD systems consisting of over a thousand atoms and successfully

* Address correspondence to mbsalmeron@lbl.gov.

Received for review July 27, 2015 and accepted September 24, 2015.

Published online September 24, 2015
10.1021/acsnano.5b04677

identified the surface ligand passivation structure of the QDs.[18]

Here we extend this approach to investigate the chemical origin of IGS in PbS QDs. One experimental challenge is the accurate measurement of the energy levels of these defect states. Traditional methods include transient photovoltage measurements, thermal admittance spectroscopy, and deep level transient spectroscopy.[8,19,20] These techniques provide quantitative information on the concentration of IGS, but cannot determine their energy levels. Photoluminescence, transient absorption, and photocurrent spectroscopies can probe the optical transitions in QD solids,[4,7,8,12,20,21] but the correlation of the various transitions with IGS is not straightforward, considering the presence of multiple intraband transitions and vibrational absorption of the organic ligands.[22] X-ray spectroscopy techniques can probe the energy level of electronic states, but the resolution is not high enough to resolve individual IGS peaks.[23−25] In fact, these spectroscopy results obtained by different groups on similar PbS QD systems vary by several 100 meV.[24,25]

We overcome this obstacle by using Kelvin probe force microscopy (KPFM) based surface potential spectroscopy (SPS)[26] to directly resolve the energetic position of the IGS. Correlation with DFT calculations and X-ray photoelectron spectroscopy (XPS) allow us to identify the source of IGS. Previously KPFM has been used to image the local work function and built-in potential in various colloidal nanomaterials.[27] However, a KPFM-based spectroscopic study on the density of states of QDs has not been reported before. Our methodology for studying defects in QDs, with more structural variability than the bulk single crystals explored by traditional surface science, is generally applicable to solution-processed materials, such as organic thin films and perovskite materials.

RESULTS AND DISCUSSION

Experimental Observation of in-Gap States. The PbS QDs studied here have an average diameter of 5.5 nm with a ∼0.9 eV band gap. As-synthesized colloidal QDs are typically capped with long insulating ligands.[18] For lead chalcogenide (PbX, X = S, Se) QDs, various ligand exchange processes have been explored to reduce interparticle distance and enable electron conduction in a QD solid. Here we explore treatments with 1,2-ethanedithiol (EDT), 3-mercaptopropionic acid (MPA), and hydrazine (HYD) that have been reported to produce ambipolar QD field effect transistors (FETs). The resulting QDs are labeled PbS-EDT, PbS-MPA, and PbS-HYD, respectively.

To study the IGS, in our previous work we performed scanning tunneling spectroscopy on individual PbS-EDT QDs deposited on indium tin oxide (ITO) substrate to obtain their electronic density of states (DOS).[13] A heterogeneous distribution of DOS was observed on measurements over tens of QDs, with about half of them showing IGS. These states are located 0.05−0.1 eV above the Fermi level and 0.15−0.3 eV above the $1S_h$ states (valence band). The actual percentage of QDs with IGS can be higher since STS is only sensitive to states localized on the top surface of the QD or with wave functions that extend all the way to the surface. The energy position of the $1S_h$ states was found to fluctuate from particle to particle, but compared to the $1S_e$ states (conduction band) they are always closer to the Fermi level. This is in agreement with the previously observed p-type doping of EDT-treated lead chalcogenide QDs.[28,29]

Here we focus on another way to measure the energy level of IGS, KPFM,[26,30] which probes the change of surface potential as a function of gate bias in a QD monolayer FET. Since the occupation of states is electrostatically tuned by the gate bias in the FET, we can use KPFM to extract the density of states. In a simple electrostatic model based on the planar capacitor geometry made by the gate and the QD monolayer, the charge density in the QDs can be obtained from the measured surface potential relative to the gate voltage (Supporting Information (SI) 2.3). This spectroscopy method (SPS) has previously been used to analyze the IGS in organic thin films.[26,31,32] Since the lateral resolution of our KPFM setup is 20−50 nm using a normal metal-coated tip (not the QD-coated tip previously used for ∼10 nm resolution imaging[13]), the measured DOS is an average over tens of QDs and thus represents the ensemble properties of the QD solid, in contrast with STS, which measures individual QDs. Therefore, in QD systems that are typically heterogeneous in their surface chemistry and in their electronic structure, this technique provides a useful method to characterize the overall change of electronic structure with different surface chemical treatments. We can see that the DOS obtained by SPS accurately resolves the band edge of the $1S_h$ states and IGS of PbS-EDT (Figure 1A). The IGS is ∼0.2 eV higher than the $1S_h$ states, in agreement with our previous STS results.[13] We are unable to probe the DOS beyond the $1S_h$/IGS band edge due to the limited charge injection capability of the FET setup (SI 2.3). This points to the main difference between the SPS technique and the STS technique: the former is based on electrostatic interactions and only probes the states that can be statically occupied and emptied, while the later is based on the quantum tunneling of electrons and probes a large range of states that electrons can tunnel into/out of.[13,15,33,34]

It has been reported that MPA passivates the QD surface more completely than EDT.[7,8,21] Our SPS results on PbS-MPA (Figure 1B), however, reveal the presence of IGS at nearly the same level as those in the PbS-EDT, indicating that the IGS are not due to incomplete ligand passivation. We further performed SPS on

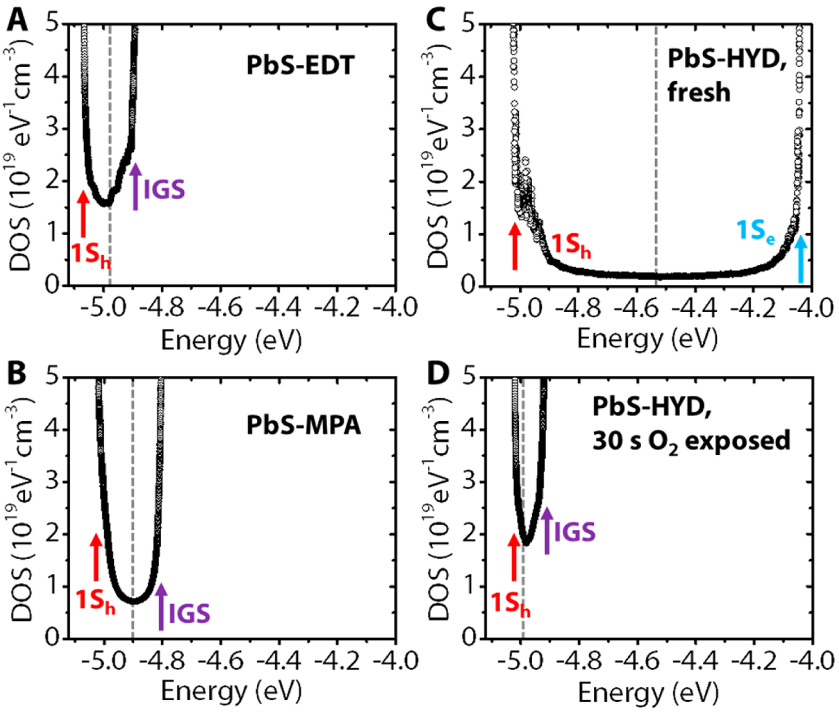

Figure 1. Experimental observation of in-gap states (IGS) near the valence band: Density of states (DOS) measured by surface potential spectroscopy of PbS QDs with different chemical treatments as labeled. Vacuum level is set to zero to align different spectra (SI 2.3). Gray dashed lines represent the position of the Fermi level at zero gate bias. All the observed IGS are empty states above the Fermi level.

PbS-HYD (Figure 1C), where the hydrazine acts as a reducing agent that was previously assumed to be able to repair surface defects of lead chalcogenide QDs.[35,36] Note that the HYD treatment was performed directly on the original oleate-coated QDs,[35] instead of on the ligand-exchanged QDs as reported before.[37] We found that PbS-HYD has a clean band gap with no observable IGS. This result suggests that the previously observed IGS may be related with adsorbed species from the environment that are removed by the hydrazine treatment. To test this assumption, we exposed the PbS-HYD QDs to air for 30 s and found that IGS reappeared at ~0.1 eV above the $1S_h$ states (Figure 1D). This suggests that either oxygen or water is at the origin of the observed IGS. As we show next by theoretical analysis and chemical spectroscopy, O_2 is the responsible species. Note that the energy levels of the $1S_h$ states of all the samples are measured to be at −5.1 to −5.0 eV (with respect to the vacuum level), in agreement with previous results for 5.5 nm PbS QDs,[38] further confirming the assignment of all the band edge states.

Theoretical Calculations on in-Gap States. In our DFT calculations we used PbS QDs of 4 nm diameter, for which we obtained a band gap of 0.94 eV. This value is slightly smaller than the experimentally observed 1.1 eV band gap for 4 nm PbS QDs,[38] due to the well-known band gap underestimation in DFT theory.[39] Nevertheless, since the calculated band gap matches that of the 5.5 nm PbS QD used in our experiments, we expect the calculated DOS to also match our experimental observations. We subsequently calculated the formation energy and electronic structure of QDs with various possible vacancies and impurities. Since the QDs are synthesized in solution, we need to consider both neutral vacancies and charged ionic vacancies (with organic counterions in the nearby solution environment). We found that neutral atomic vacancies (Pb, S, L, where L refers to ligand), neutral divacancies (PbS, PbL_2), and charged ion vacancies (Pb^{2+}, S^{2-}, L^-) have formation energies in the range 1.6−2.3, 0.8−1.8, and −0.8−1 eV, respectively. Thus, the formation of neutral atomic vacancies during QD growth in solution is very unlikely, while charged ion vacancies are most likely to form. Our calculations show that PbS and S^{2-} vacancies produce IGS near the conduction band, while all other charged ion vacancies and neutral divacancies do not induce IGS (Figure S6). This leads us to conclude that external molecules adsorbed on the QD surface are at the origin of the observed IGS. These molecules need to be small and reactive in order to adsorb on the QD surface after diffusing through the ligands. Prime candidates are water and oxygen because they are present (in trace amounts) during synthesis and during glovebox storage.

The calculations show that adsorbed water does not produce IGS (Figure S7), while adsorbed molecular oxygen produces IGS slightly above the valence band. Using the spin-polarized generalized gradient approximation (GGA), we found two unoccupied states at

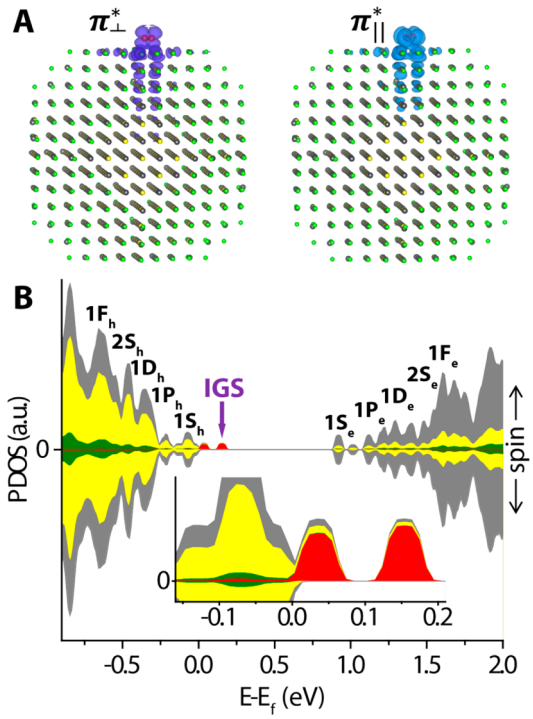

Figure 2. DFT calculation reveals that molecular oxygen is at the origin of IGS. (A) DFT-calculated probability density distribution from the wave function of the two unoccupied IGS derived from O_2 adsorbed on a 4 nm PbS QD surface. These states are formed by hybridization of the oxygen $\pi^*_\perp$ and $\pi^*_{||}$ orbitals with the $1S_h$ state of the QD. (B) DFT-calculated spin-polarized partial density of states (PDOS) for PbS QD with one adsorbed O_2 molecule in the GGA approximation. The contributions from different elements are shown in color (Pb: gray, S: yellow, Cl: green, O: red). E_f refers to the Fermi level. There are two empty IGS at 0.07 eV ($\pi^*_\perp$) and 0.18 eV ($\pi^*_{||}$) above the $1S_h$ state due to triplet states of O_2. Inset: Expanded view of the IGS and $1S_h$ states.

0.07 and 0.18 eV above the $1S_h$ state (Figure 2). A higher level hybrid functional imposes a 0.13 eV correction on these states, shifting them up to 0.20 and 0.31 eV above $1S_h$ (SI 3.8). The energies of these states match those of the experimentally observed IGS in PbS-EDT, PbS-MPA, and the 30 s air exposed PbS-HYD. The two empty O_2-derived IGS are formed by coupling of the two unoccupied π^* orbitals of molecular oxygen with the $1S_h$ state of the QD. The wave function density of the two IGS extends deep into the QD (Figure 2A). At the center, the wave function density still has a finite value that is 1.07% of the maximum density inside the QD. Accordingly to the Bader charge analysis of the total charge density, a partial electron transfer of 0.33 e^- occurs from the QD to the oxygen molecule. The O—O distance in the adsorbed O_2 is 1.278 Å, a slight increase compared to the free molecule value (1.241 Å). The calculated formation energy of the oxygen on the QD surface is −0.32 eV (Table 1), in contrast with the positive formation energies of various vacancy defects. Since the van der Waals interaction was not taken into account in the calculation, the actual formation energy can be lower (larger in absolute value) than −0.32 eV. The surface ligand species and their distribution may also affect the absolute values of the formation energy. However, we expect the relative formation energy difference between different adsorption species to be reasonable.

TABLE 1. Formation Energy and Presence of IGS of Possible Adsorbed Molecules on a PbS QD

adsorbate	formation energy (eV)	presence of IGS
O_2	−0.32	yes
2 O_2	−0.22	yes
2 O (dissociated)	−2.36	no
S→O (surf)[a]	−1.08	no
H_2O	−0.78	no

[a] Substitutional atomic defect where an oxygen atom replaces a sulfur atom on the QD surface.

We calculated also the DOS when oxygen molecules are dissociated on the QD surface (in minimum energy configuration) and found that no IGS are created in that case (Figure S8). Furthermore, substitutional atomic oxygen defects (where an oxygen atom replaces a sulfur atom, both at the surface and interior) were found to not produce IGS either. Therefore, among the theoretically calculated intrinsic and external defects, only molecular oxygen produces IGS with energy levels matching the experimental results.

Spectroscopic Evidence and Further Theoretical Support on the Origin of IGS. To confirm the existence and analyze the concentration of molecular oxygen, we performed X-ray photoelectron spectroscopy, targeting the O 1s emission peak (Figure 3). All the samples shown in Figure 1 were measured except PbS-MPA, where the ligand contains oxygen (thus complicating the spectra). XPS confirms the existence of O_2 (533.9 eV) on PbS-EDT.[40] Another peak at 532.1 eV corresponds to the −COO− groups, likely arising from the residual unexchanged oleate ligands.[18] In PbS-HYD QDs, in contrast, O_2 species are absent. When exposed to 1 atm of a 25% O_2/75% Ar gas mixture for 30 s, the 533.9 eV O_2 peak appeared on the PbS-HYD. The 531.3 eV peak corresponds to −OH groups that were present on the oleate-passivated QDs[18] and not fully removed by the HYD treatment. Peak area analysis shows that the concentration of O_2 on PbS-EDT and on the 30 s exposed PbS-HYD is roughly similar, approximately 10 molecules per QD on average (SI 4.2). The amount of O_2 on PbS-HYD remained constant after a 10 min exposure (although the amount of atomic oxygen species increased) (Figure S10). The correlation of the presence or absence of O_2 with the formation of IGS, together with the theoretical results on the effect of O_2 in producing the IGS, lends strong support to our conclusion on the origin of the IGS. It should be noted that the XPS spectral resolution is limited by the small amount of oxygen species present on the QDs, and the resolution on the PbS-EDT sample is slightly worse than on the PbS-HYD

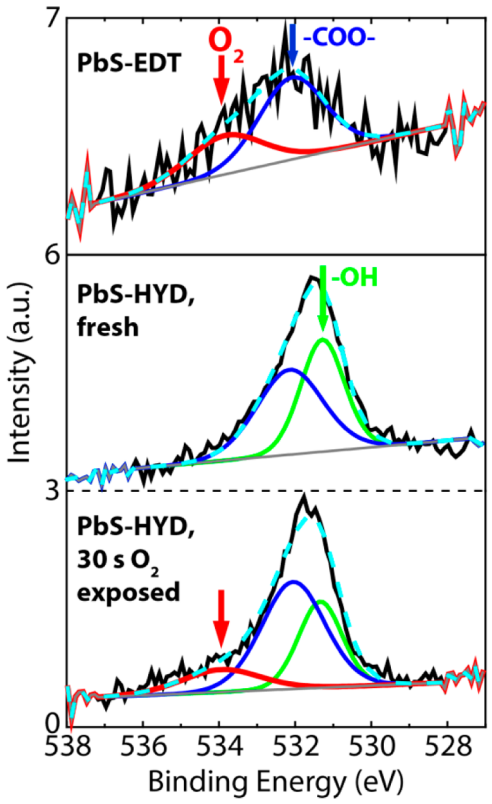

Figure 3. X-ray photoelectron spectroscopy showing the presence/absence of adsorbed O_2 on QDs with/without IGS. O 1s XPS peaks from PbS-EDT (intensity is 3 times expanded), PbS-HYD, and PbS-HYD exposed for 30 s to a 1 atm 25% O_2/75% Ar gas mixture. Three components are used for the fit. Each component has the same peak position and width for the three samples. The red peak component at 533.9 eV corresponds to O_2, while the component at 532.1 eV (blue) and that at 531.3 eV (green) are assigned to −COO− and −OH species, respectively.

due to the presence of ligands in the former. Also note that the existence of ~10 O_2 per QD is not contradictory to the STS results, where IGS was observed on only *ca.* half of the QDs,[13] since the O_2 not located under the STM tip may not be sensed by STS, as explained before.

Since more than one O_2 molecule can be present on each QD, we further performed calculations on the effect of two O_2 molecules absorbed on two opposite {100} facets. The wave functions of the IGS induced by the two molecules are symmetric and have a very small overlap at the center (Figure 4A). The IGS wave function density at the center of the QD is 1.24% of the maximum density inside the QD, slightly larger than the case of single O_2. Using the GGA approximation we obtained the DOS shown in Figure 4B. Four states appear inside the band gap, with two spin-up states (0.05 and 0.16 eV above the $1S_h$ state) and two spin-down states (0.06 and 0.18 eV above the $1S_h$ state). We can see that in the case of two O_2 the IGS induced by each O_2 resembles that of the IGS of single O_2 on the QD. Similar to the single O_2 case, using the higher level hybrid functional we expect the same 0.13 eV upshift in energy in the two O_2 case, resulting in four states between 0.18 and 0.31 eV above the $1S_h$ state. We thus expect that the energy level of the IGS in the case of multiple O_2 on one QD will not change significantly as long as these states are not strongly coupled.

With two O_2 on the QD, charge transfer from QD to each of the O_2 molecules estimated from Bader charge analysis decreases to 0.30 e^- per molecule. This is because the QD is resistant to more electron withdrawal. As a result, the formation energy increases to −0.22 eV per molecule. With more O_2 on the QD, we expect a further increase of formation energy. This might be the reason that the amount of O_2 saturates after the PbS-HYD was exposed to oxygen for only 30 s (as shown by XPS). The formation energies of various possible impurity defects are shown in Table 1. Molecular oxygen has the largest formation energy (smallest in absolute value) among the considered impurities and is the only one that produces IGS. We need to note that prolonged oxidation of PbS QDs results in the formation of various oxide species such as $PbSO_3$ and $PbSO_4$.[41] In that case the simple vacancy and impurity defect picture is not sufficient to describe the electronic structure of the QD, since the composition is significantly modified.

Further Discussions. We have considered various possible defects that can form during the solution phase synthesis process, which is the first step of all the device fabrication based on colloidal QDs. Among these defects, molecular oxygen, an unintentional impurity that is hard to avoid, is found to be the most likely source of IGS near the valence band. Various postsynthetic treatments, on the other hand, can modify the amount and/or type of defects, thus changing the IGS. The hydrazine treatment shown here is one example of removing O_2 and eliminating IGS. Another postsynthesis approach of electronic modification is stoichiometry control *via* deposition of excess lead or chalcogen.[42,43] Although neutral atomic vacancies are unlikely to form during solution synthesis (as discussed before), this postsynthesis control can produce QDs with excess Pb or S (*i.e.*, QD with neutral S or Pb vacancies). According to previous calculations[8,16] and our own DFT results (not shown here), neutral Pb vacancies produce IGS near the valence band, while neutral S or L (ligand) vacancies produce IGS near the conduction band.

The intrinsic defect physics of lead chalcogenide QDs can be understood in the general scheme of ionic semiconductors. Similar to methylammonium lead iodide perovskite systems,[44] charge-balanced (surface fully passivated by ligands) PbS QDs do not show IGS. This has been demonstrated by DFT calculations on PbS QDs passivated with oleic acid and hydroxyl groups,[18] with EDT,[16] and with MPA + Cl.[8] All the above ligands form ionic bonds with the surface Pb^{2+}, thus maintaining the overall stoichiometry of the Pb-rich QD.[45−47] In our work, to make DFT calculations

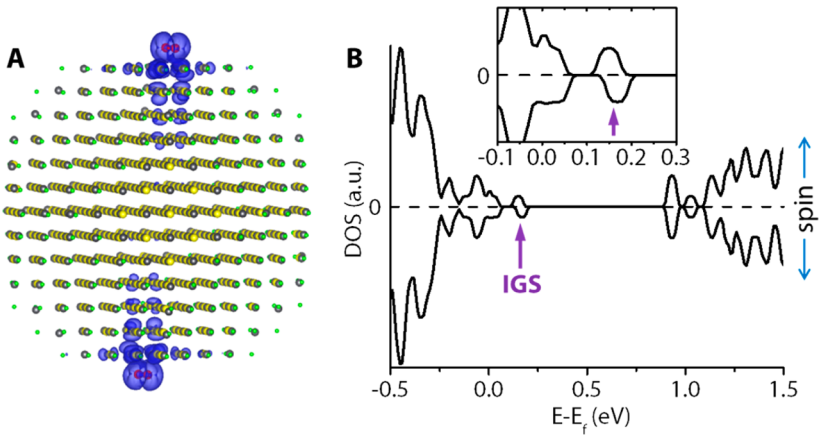

Figure 4. DFT calculations of two O_2 molecules on a PbS quantum dot. (A) Integrated probability density distribution of the states between E_f and $E_f + 0.25$ eV. (B) Calculated spin-polarized DOS in the GGA approximation. The inset is an expanded view of the IGS. Four IGS are present at 0.05 eV ($\pi^*_\perp$) and 0.16 eV ($\pi^*_\parallel$) above the $1S_h$ state (spin-up) and at 0.06 eV ($\pi^*_\perp$) and 0.18 eV ($\pi^*_\parallel$) above the $1S_h$ state (spin-down).

possible on a QD as large as 4 nm, we used Cl as the passivation ligand and found a clean band gap after complete passivation. As long as the ligands form ionic bonds with Pb, different ligand species are expected to have similar effects on IGS properties. This is in agreement with our experimental results, where similar IGS were found on QDs with three different chemical treatments (EDT, MPA, and HYD+O_2).

As explained before, as-synthesized QDs in solution tend to not have neutral defects due to their large formation energy. To fabricate electronically active devices, however, the QD solids typically need to go through a ligand exchange process,[7,8] which can result in a loss of ligands, leading to QDs with excess cation atoms (Pb in our case). These neutral vacancy defects, if present, will induce IGS near the conduction band. However, the fact that we do not observe n-type IGS indicates that either our QDs are well passivated by ligands (*i.e.*, there is no ligand vacancy) or the IGS induced by ligand vacancies are too close (within ~50 meV) to the conduction band to be observed. In either case, O_2 remains the only experimentally observable deep IGS in typical ligand-exchanged QD solids that can be detrimental to optoelectronic devices.

It has previously been found that oxygen exposure can induce p-type doping in lead chalcogenide QDs,[48−50] supporting the O_2-induced IGS mechanism. Moreover, these QD solids with various ligand treatments (EDT, *n*-butylamine, MPA, *etc.*) exhibit unintentional p-type doping even in inert atmosphere, with carrier densities of $10^{16}-10^{17}$ cm^{-3} for QDs of 5−6 nm diameter.[42,51,52] This doping effect is also mainly due to the IGS produced by O_2, whose surface concentration on the QD is limited by the energy cost of the charge transfer from the QD to the adsorbed O_2 (as explained above). From our STS results on the PbS-EDT we obtain an average Fermi level (E_f)−$1S_h$ state (E_v) separation of 0.15 eV (averaged over the QDs with observable IGS, since those without IGS tend to have $1S_h$ states far from the Fermi level and are thus electronically inactive). The estimated effective density of valence band states for our 5.5 nm PbS QD solids is $n_v = 2.1 \times 10^{19}$ cm^{-3} (see Methods). Thus, at room temperature the hole carrier density can be calculated as[1]

$$p = n_v \exp\left(-\frac{E_f - E_v}{kT}\right) = 6.4 \times 10^{16}\ \text{cm}^{-3}$$

in good agreement with previous results. This quantitative agreement reveals that our proposed IGS mechanism is generally applicable to lead chalcogenide QDs, where unintentional doping can be induced by surface-saturated O_2.

CONCLUSION

We have identified molecular oxygen as the dominant source of IGS in colloidal PbS quantum dots. The in-gap electronic structure of the QDs is immune to most of the charged ion vacancies that may form during the synthesis process. To engineer IGS-free QDs for optoelectronic applications, we need to first reduce the surface oxygen during the postsynthesis treatment process and ideally also fully passivate the surface with ligands that can block the readsorption of O_2 on QDs.[10,11]

METHODS

Synthesis of PbS quantum dots was done following a previously reported procedure.[53] QD size and morphology were measured by transmission electron microscopy, while their band gap is determined by UV−vis absorption spectroscopy. QD monolayers were prepared by spin-coating colloidal QDs on a substrate followed by chemical treatments and solvent washing to obtain a monolayer with different ligands or different

surface chemistry. The species of the surface ligands were characterized by Fourier transform infrared spectroscopy measurements. All of the sample preparation procedures were done in an Ar glovebox with <1 ppm oxygen. Sample transfer to the measurement chambers of KPFM, STM, and XPS was done using a nitrogen glovebag or portable vacuum chamber. During the whole sample preparation, transfer, and measurement process the sample was never exposed to air.

STM measurements were performed with a home-built system operated at 77 K in ultrahigh vacuum. The differential conductance (d*I*/d*V*) spectra were measured using a lock-in technique with fixed tip to sample distance. The electronic structure of the tip was checked by recording background spectra on the bare ITO substrate, before and after measuring the STS spectra of each QD.

KPFM was done using a home-built setup that operates in single-pass, frequency feedback, noncontact mode. The AFM tip used to simultaneously probe the topography and surface potential is silicon coated with Ti/Pt, with a typical tip radius of ~28 nm.

DFT calculations were carried out using the Vienna Ab Initio Simulation Package (VASP), using the generalized gradient approximation (GGA) functional (PW91) and a hybrid functional (HSE03).

XPS was done on thin-film samples deposited on Au. The O 1s peak energy was calibrated by the Pb 4f peak. Gaussian–Lorentzian peak fitting was performed by fixing the peak energy and width of each component to be the same, for all four samples (PbS-EDT, PbS-HYD, 30 s exposed PbS-HYD, 10 min exposed PbS-HYD). Concentration of the O_2 species was estimated by comparing the O 1s and the Pb 4f peak areas and considering the atomic sensitivity factor and geometric factors.

The effective density of hole states is estimated using

$$n_v = 8/V_{eff}$$

considering that the valence band of PbS QDs is 8-fold degenerate.[54] V_{eff} is the effective average volume occupied by each QD. Assuming that the QDs have a spherical shape, with a volume fill fraction of 0.5 and an inter-QD distance of 1.6 nm for PbS-EDT,[51] we have $V_{eff} = 3.75 \times 10^{-19}$ cm^3. Thus, $n_v = 2.1 \times 10^{19}$ cm^{-3}.

Conflict of Interest: The authors declare no competing financial interest.

Acknowledgment. This work was supported by the "Self-Assembly of Organic/Inorganic Nanocomposite Materials" program, Office of Science, the Office of Basic Energy Sciences (BES), Materials Sciences and Engineering (MSE) Division of the U.S. Department of Energy (DOE) under Contract No. DE-AC02-05CH11231. It used resources of the Molecular Foundry, a DOE Office of Science user facility. Computations used resources of the National Energy Research Scientific Computing Center and Oak Ridge Leadership Computing Facility, which are DOE Office of Science user facilities, with the computational time allocated by the Innovative and Novel Computational Impact on Theory and Experiment (INCITE) project. S.B. acknowledges fellowship support by the European Union under FP7-PEOPLE-2012-IOF-327581. L.L. acknowledges support from the Alexander van Humboldt Foundation.

Supporting Information Available: The Supporting Information is available free of charge on the ACS Publications website at DOI: 10.1021/acsnano.5b04677.

Materials and methods; surface potential spectroscopy; density functional theory calculations; X-ray photoelectron spectroscopy (PDF)

REFERENCES AND NOTES

1. Sze, S. M. *Physics of Semiconductor Devices*, 2nd ed.; Wiley: New York, 1981.
2. Queisser, H. J.; Haller, E. E. Defects in Semiconductors: Some Fatal, Some Vital. *Science* **1998**, *281*, 945–950.
3. Rurali, R. Colloquium: Structural, Electronic, and Transport Properties of Silicon Nanowires. *Rev. Mod. Phys.* **2010**, *82*, 427–449.
4. Nagpal, P.; Klimov, V. I. Role of Mid-Gap States in Charge Transport and Photoconductivity in Semiconductor Nanocrystal Films. *Nat. Commun.* **2011**, *2*, 486.
5. Wolkin, M. V.; Jorne, J.; Fauchet, P. M.; Allan, G.; Delerue, C. Electronic States and Luminescence in Porous Silicon Quantum Dots: the Role of Oxygen. *Phys. Rev. Lett.* **1999**, *82*, 197.
6. Cordones, A. A.; Scheele, M.; Alivisatos, A. P.; Leone, S. R. Probing the Interaction of Single Nanocrystals with Inorganic Capping Ligands: Time-Resolved Fluorescence from CdSe-CdS Quantum Dots Capped With Chalcogenidometalates. *J. Am. Chem. Soc.* **2012**, *134*, 18366–18373.
7. Tang, J.; Kemp, K. W.; Hoogland, S.; Jeong, K. S.; Liu, H.; Levina, L.; Furukawa, M.; Wang, X.; Debnath, R.; Cha, D.; et al. Colloidal-Quantum-Dot Photovoltaics Using Atomic-Ligand Passivation. *Nat. Mater.* **2011**, *10*, 765–771.
8. Ip, A. H.; Thon, S. M.; Hoogland, S.; Voznyy, O.; Zhitomirsky, D.; Debnath, R.; Levina, L.; Rollny, L. R.; Carey, G. H.; Fischer, A.; et al. Hybrid Passivated Colloidal Quantum Dot Solids. *Nat. Nanotechnol.* **2012**, *7*, 577–582.
9. Carey, G. H.; Levina, L.; Comin, R.; Voznyy, O.; Sargent, E. H. Record Charge Carrier Diffusion Length in Colloidal Quantum Dot Solids via Mutual Dot-To-Dot Surface Passivation. *Adv. Mater.* **2015**, *27*, 3325–3330.
10. Ning, Z.; Voznyy, O.; Pan, J.; Hoogland, S.; Adinolfi, V.; Xu, J.; Li, M.; Kirmani, A. R.; Sun, J.-P.; Minor, J.; et al. Air-Stable N-Type Colloidal Quantum Dot Solids. *Nat. Mater.* **2014**, *13*, 822–828.
11. Chuang, C. M.; Brown, P. R.; Bulović, V.; Bawendi, M. G. Improved Performance and Stability in Quantum Dot Solar Cells Through Band Alignment Engineering. *Nat. Mater.* **2014**, *13*, 796–801.
12. Chuang, C.-H. M.; Maurano, A.; Brandt, R. E.; Hwang, G. W.; Jean, J.; Buonassisi, T.; Bulović, V.; Bawendi, M. G. Open-Circuit Voltage Deficit, Radiative Sub-Bandgap States, and Prospects in Quantum Dot Solar Cells. *Nano Lett.* **2015**, *15*, 3286–3294.
13. Zhang, Y.; Zherebetskyy, D.; Bronstein, N. D.; Barja, S.; Lichtenstein, L.; Schuppisser, D.; Wang, L. W.; Alivisatos, A. P.; Salmeron, M. Charge Percolation Pathways Guided by Defects in Quantum Dot Solids. *Nano Lett.* **2015**, *15*, 3249–3253.
14. Zhang, Y.; Chen, Q.; Alivisatos, A. P.; Salmeron, M. Dynamic Charge Carrier Trapping in Quantum Dot Field Effect Transistors. *Nano Lett.* **2015**, *15*, 4657–4663.
15. Diaconescu, B.; Padilha, L. A.; Nagpal, P.; Swartzentruber, B. S.; Klimov, V. I. Measurement of Electronic States of PbS Nanocrystal Quantum Dots using Scanning Tunneling Spectroscopy: the Role of Parity Selection Rules in Optical Absorption. *Phys. Rev. Lett.* **2013**, *110*, 127406.
16. Kim, D.; Kim, D.-H.; Lee, J.-H.; Grossman, J. C. Impact of Stoichiometry on the Electronic Structure of PbS Quantum Dots. *Phys. Rev. Lett.* **2013**, *110*, 196802.
17. Voznyy, O.; Thon, S. M.; Ip, A. H.; Sargent, E. H. Dynamic Trap Formation and Elimination in Colloidal Quantum Dots. *J. Phys. Chem. Lett.* **2013**, *4*, 987–992.
18. Zherebetskyy, D.; Scheele, M.; Zhang, Y.; Bronstein, N.; Thompson, C.; Britt, D.; Salmeron, M.; Alivisatos, P.; Wang, L.-W. Hydroxylation of the Surface of PbS Nanocrystals Passivated with Oleic Acid. *Science* **2014**, *344*, 1380–1384.
19. Bozyigit, D.; Jakob, M.; Yarema, O.; Wood, V. Deep Level Transient Spectroscopy (DLTS) on Colloidal-Synthesized Nanocrystal Solids. *ACS Appl. Mater. Interfaces* **2013**, *5*, 2915–2919.
20. Bozyigit, D.; Volk, S.; Yarema, O.; Wood, V. Quantification of Deep Traps in Nanocrystal Solids, Their Electronic Properties, and Their Influence on Sevice Behavior. *Nano Lett.* **2013**, *13*, 5284–5288.
21. Jeong, K. S.; Tang, J.; Liu, H.; Kim, J.; Schaefer, A. W.; Kemp, K.; Levina, L.; Wang, X.; Hoogland, S.; Debnath, R.; et al. Enhanced mobility-lifetime products in PbS colloidal quantum dot photovoltaics. *ACS Nano* **2012**, *6*, 89–99.
22. Pandey, A.; Guyot-Sionnest, P. Slow Electron Cooling in Colloidal Quantum Dots. *Science* **2008**, *322*, 929–932.

23. Katsiev, K.; Ip, A. H.; Fischer, A.; Tanabe, I.; Zhang, X.; Kirmani, A. R.; Voznyy, O.; Rollny, L. R.; Chou, K. W.; Thon, S. M.; et al. The Complete In-Gap Electronic Structure of Colloidal Quantum Dot Solids and Its Correlation with Electronic Transport and Photovoltaic Performance. *Adv. Mater.* **2014**, *26*, 937–942.
24. Brown, P. R.; Kim, D.; Lunt, R. R.; Zhao, N.; Bawendi, M. G.; Grossman, J. C.; Bulović, V. Energy Level Modification in Lead Sulfide Quantum Dot Thin Films Through Ligand Exchange. *ACS Nano* **2014**, *8*, 5863–5872.
25. Axnanda, S.; Scheele, M.; Crumlin, E. J.; Mao, B.; Chang, R.; Rani, S.; Faiz, M.; Wang, S.; Alivisatos, A. P.; Liu, Z. Direct Work Function Measurement by Gas Phase Photoelectron Spectroscopy and Its Application on PbS Nanoparticles. *Nano Lett.* **2013**, *13*, 6176–6182.
26. Zhang, Y.; Ziegler, D.; Salmeron, M. Charge Trapping States at the SiO_2-Oligothiophene Monolayer Interface in Field Effect Transistors Studied by Kelvin Probe Force Microscopy. *ACS Nano* **2013**, *7*, 8258–8265.
27. Nanayakkara, S. U.; van de Lagemaat, J.; Luther, J. M. Scanning Probe Characterization of Heterostructured Colloidal Nanomaterials. *Chem. Rev.* **2015**, *115*, 8157–8181.
28. Luther, J. M.; Law, M.; Beard, M. C.; Song, Q.; Reese, M. O.; Ellingson, R. J.; Nozik, A. J. Schottky Solar Cells Based on Colloidal Nanocrystal Films. *Nano Lett.* **2008**, *8*, 3488–3492.
29. Barkhouse, A. R.; Pattantyus-Abraham, A. G.; Levina, L.; Sargent, E. H. Thiols Passivate Recombination Centers in Colloidal Quantum Dots Leading to Enhanced Photovoltaic Device Efficiency. *ACS Nano* **2008**, *2*, 2356–2362.
30. Zhang, Y.; Pluchery, O.; Caillard, L.; Lamic-Humblot, A.; Casale, S.; Chabal, Y. J.; Salmeron, M. Sensing the Charge State of Single Gold Nanoparticles via Work Function Measurements. *Nano Lett.* **2015**, *15*, 51–55.
31. Celebi, K.; Jadhav, P. J.; Milaninia, K. M.; Bora, M.; Baldo, M. A. The Density of States in Thin Film Copper Phthalocyanine Measured by Kelvin Probe Force Microscopy. *Appl. Phys. Lett.* **2008**, *93*, 083308.
32. Tal, O.; Rosenwaks, Y.; Preezant, Y.; Tessler, N.; Chan, C. K.; Kahn, A. Direct Determination of the Hole Density of States in Nndoped and Doped Amorphous Organic Films with High Lateral Resolution. *Phys. Rev. Lett.* **2005**, *95*, 256405.
33. Liljeroth, P.; Overgaag, K.; Urbieta, A.; Grandidier, B.; Hickey, S. G.; Vanmaekelbergh, D. *Phys. Rev. Lett.* **2005**, *95*, 086801.
34. Overgaag, K.; Liljeroth, P.; Grandidier, B.; Vanmaekelbergh, D. Scanning Tunneling Spectroscopy of Individual PbSe Quantum Dots and Molecular Aggregates Stabilized in an Inert Nanocrystal Matrix. *ACS Nano* **2008**, *2*, 600–606.
35. Talapin, D. V.; Murray, C. B. PbSe Nanocrystal Solids for N- and P-Channel Thin Film Field-Effect Transistors. *Science* **2005**, *310*, 86–89.
36. Koh, W.; Koposov, A. Y.; Stewart, J. T.; Pal, B. N.; Robel, I.; Pietryga, J. M.; Klimov, V. I. Heavily Doped n-type PbSe and PbS Nanocrystals Using Ground-State Charge Transfer from Cobaltocene. *Sci. Rep.* **2013**, *3*, 2004.
37. Semonin, O. E.; Luther, J. M.; Choi, S.; Chen, H.-Y.; Gao, J.; Nozik, A. J.; Beard, M. C. Peak External Photocurrent Quantum Efficiency Exceeding 100% via MEG in a Quantum Dot Solar Cell. *Science* **2011**, *334*, 1530–1533.
38. Jasieniak, J.; Califano, M.; Watkins, S. E. Size-Dependent Valence and Conduction Band-Edge Energies of Semiconductor Nanocrystals. *ACS Nano* **2011**, *5*, 5888–5902.
39. Perdew, J. P. Density Functional Theory and the Band Gap Problem. *Int. J. Quantum Chem.* **1986**, *19*, 497–523.
40. Shuxian, Z.; Hall, W. K.; Ertl, G.; Knözinger, H. X-ray Photoemission Study of Oxygen and Nitric Oxide Adsorption on MoS_2. *J. Catal.* **1986**, *100*, 167–175.
41. Tang, J.; Brzozowski, L.; Barkhouse, D. A. R.; Wang, X.; Debnath, R.; Wolowiec, R.; Palmiano, E.; Levina, L.; Pattantyus-Abraham, A. G.; Jamakosmanovic, D.; et al. Quantum Dot Photovoltaics in the Extreme Quantum Confinement Regime: the Surface-Chemical Origins of Exceptional Air- and Light-Stability. *ACS Nano* **2010**, *4*, 869–878.
42. Oh, S. J.; Berry, N. E.; Choi, J.-H.; Gaulding, E. A.; Paik, T.; Hong, S.-H.; Murray, C. B.; Kagan, C. R. Stoichiometric Control of Lead Chalcogenide Nanocrystal Solids to Enhance Their Electronic and Optoelectronic Device Performance. *ACS Nano* **2013**, *7*, 2413–2421.
43. Oh, S. J.; Berry, N. E.; Choi, J.-H.; Gaulding, E. A.; Lin, H.; Paik, T.; Diroll, B. T.; Muramoto, S.; Murray, C. B.; Kagan, C. R. Designing High-Performance PbS and PbSe Nanocrystal Electronic Devices Through Stepwise, Post-Synthesis, Colloidal Atomic Layer Deposition. *Nano Lett.* **2014**, *14*, 1559–1566.
44. Kim, J.; Lee, S.-H.; Lee, J. H.; Hong, K.-H. The Role of Intrinsic Defects in Methylammonium Lead Iodide Perovskite. *J. Phys. Chem. Lett.* **2014**, *5*, 1312–1317.
45. Owen, J. The Coordination Chemistry of Nanocrystal Surfaces. *Science* **2015**, *347*, 615–616.
46. Moreels, I.; Lambert, K.; De Muynck, D.; Vanhaecke, F.; Poelman, D.; Martins, J. C.; Allan, G.; Hens, Z. Composition and Size-Dependent Extinction Coefficient of Colloidal PbSe Quantum Dots. *Chem. Mater.* **2007**, *19*, 6101–6106.
47. Choi, H.; Ko, J.-H.; Kim, Y.-H.; Jeong, S. Steric-Hindrance-Driven Shape Transition in PbS Quantum Dots: Understanding Size-Dependent Stability. *J. Am. Chem. Soc.* **2013**, *135*, 5278–5281.
48. Leschkies, K. S.; Kang, M. S.; Aydil, E. S.; Norris, D. J. Influence of Atmospheric Gases on the Electrical Properties of PbSe Quantum-Dot Films. *J. Phys. Chem. C* **2010**, *114*, 9988–9996.
49. Zhao, N.; Osedach, T. P.; Chang, L.-Y.; Geyer, S. M.; Wanger, D.; Binda, M. T.; Arango, A. C.; Bawendi, M. G.; Bulovic, V. *ACS Nano* **2010**, *4*, 3743–3752.
50. Zarghami, M. H.; Liu, Y.; Gibbs, M.; Gebremichael, E.; Webster, C.; Law, M. P-Type PbSe and PbS Quantum Dot Solids Prepared with Short-Chain Acids and Diacids. *ACS Nano* **2010**, *4*, 2475–2485.
51. Klem, E. J. D.; Shukla, H.; Hinds, S.; MacNeil, D. D.; Levina, L.; Sargent, E. H. Impact of Dithiol Treatment and Air Annealing on the Conductivity, Mobility, and Hole Density in PbS Colloidal Quantum Dot Solids. *Appl. Phys. Lett.* **2008**, *92*, 212105.
52. Gao, J.; Luther, J. M.; Semonin, O. E.; Ellingson, R. J.; Nozik, A. J.; Beard, M. C. Quantum Dot Size Dependent J-V Characteristics in Heterojunction ZnO/PbS Quantum Dot Solar Cells. *Nano Lett.* **2011**, *11*, 1002–1008.
53. Hines, M. A.; Scholes, G. D. Colloidal PbS Nanocrystals with Size-Tunable Near-Infrared Emission: Observation of Post-Synthesis Self-Narrowing of the Particle Size Distribution. *Adv. Mater.* **2003**, *15*, 1844–1849.
54. Kang, I.; Wise, F. W. Electronic Structure and Optical Properties of PbS and PbSe Quantum Dots. *J. Opt. Soc. Am. B* **1997**, *14*, 1632–1646.